Charge lifetime measurements at high average current using a K_2CsSb photocathode inside a dc high voltage photogun

R. R. Mammei,* R. Suleiman, J. Feingold, P. A. Adderley, J. Clark, S. Covert, J. Grames, J. Hansknecht, D. Machie, and M. Poelker

Thomas Jefferson National Accelerator Facility, Newport News, Virginia 23606, USA

T. Rao, J. Smedley, and J. Walsh

Brookhaven National Laboratory, Upton, New York 11973, USA

J. L. McCarter

Department of Physics, University of Virginia, Charlottesville, Virginia 22901, USA

M. Ruiz-Osés

Stony Brook University, Stony Brook, New York 11794, USA

(Received 16 August 2012; published 13 March 2013)

Two K_2CsSb photocathodes were manufactured at Brookhaven National Lab and delivered to Jefferson Lab within a compact vacuum apparatus at pressure $\sim 10^{-11}$ Torr. These photocathodes were evaluated using a dc high voltage photogun biased at voltages up to 200 kV, and illuminated with laser light at wavelengths 440 or 532 nm, to generate dc electron beams at currents up to 20 mA. Some conditions produced exceptionally large photocathode charge lifetimes, without measurable quantum efficiency decay, even from the center of the photocathode where operation using GaAs photocathodes is precluded due to ion bombardment. Under other conditions the charge lifetime was poor due to extensive ion bombardment under severely degraded vacuum conditions, and as a result of localized heating via the laser beam. Following beam delivery, the photocathodes were evaluated using a scanning electron microscope to determine surface morphology.

DOI: 10.1103/PhysRevSTAB.16.033401 PACS numbers: 29.25.Bx, 29.27.Fh, 79.60.−i, 52.59.Sa

I. INTRODUCTION

There are two popular photocathode choices for generating high average current electron beams at accelerators using relatively inexpensive rf-pulsed green-laser light: GaAs and K_2CsSb. The GaAs photocathode can exhibit very high quantum efficiency (QE) and it can produce a beam with small thermal emittance [1], but it is widely recognized to be a very fragile photocathode requiring strict adherence to procedures that maintain cleanliness of the photocathode surface on an atomic scale. Once inside the photogun, it is prone to rapid QE loss that can result from many situations including poor vacuum, high voltage discharges within the gun, and low level field emission. The K_2CsSb photocathode can exhibit high QE, but whereas GaAs can be purchased from numerous reliable vendors, K_2CsSb is a compound ''grown'' by the user near the gun, by successive application of elemental species on a suitable substrate. Consistent results depend on adherence to proper growth procedures. The K_2CsSb photocathode has a slightly larger thermal emittance [2] compared to GaAs but it is considered to be a prompt emitter because of its positive-electron affinity (PEA) nature, producing shorter bunches than GaAs. The biggest advantage however is the photocathode's ability to survive under markedly harsher vacuum conditions compared to GaAs [3].

The basis for these introductory comments stems from reports of accelerator operation at a handful of locations [4–8]. Notably, the Jefferson Lab (JLab) free electron laser (FEL) employs GaAs inside a dc high voltage photogun biased at 350 kV and routinely operates at 5 mA average current [8], although occasional high voltage discharges sometimes necessitate time consuming photocathode replacement. The Boeing FEL used K_2CsSb inside a normal conducting rf gun and produced a maximum average current of 32 mA [3]. The photocathode provided high QE and was very robust, surviving inside a vacuum chamber known to have a leak to the water cooling jacket of the photogun. QE would decrease during operation but could be restored to 100% of its original value by application of more cesium. The Cornell University photogun group recently set impressive new milestones using both of these

*Corresponding author.
rmammei@jlab.org

photocathodes by demonstrating sustained delivery of 20 mA average current for 8 hours from K_2CsSb [9] with no observed QE decay and 50 mA for several minutes using GaAs with a 100 C charge lifetime [10].

The purpose of this work was to compare the performance of the K_2CsSb photocathode inside a dc high voltage photogun that had been used extensively to characterize GaAs performance [11]. Under nominally identical conditions (gun and beam line vacuum, drive laser wavelength and laser spot size, etc.), the performance of the two photocathodes can be quantitatively assessed. The following observations will be described in detail in sections that follow.

K_2CsSb photocathodes can be manufactured at one location and delivered to the photogun many miles away under UHV conditions, without appreciable QE decay.

Under UHV conditions ($< 10^{-11}$ Torr), the lifetime of the K_2CsSb photocathode does not appear to be significantly affected by ion bombardment. However, under degraded vacuum conditions ($\sim 10^{-9}$ Torr) ion bombardment was a serious problem that led to the complete removal of the photocathode material from the substrate.

Under UHV conditions ($< 10^{-11}$ Torr), the QE of the K_2CsSb photocathode was most strongly dependent on laser heating.

The geometric normalized rms emittance of the photocathode, before and after sustained use, was comparable to reported values.

Scanning electron microscope (SEM) measurements indicate significant morphological changes associated with use.

II. EXPERIMENT

A. Photocathode preparation

Two K_2CsSb photocathodes were manufactured at Brookhaven National Lab (BNL) inside an ultrahigh vacuum deposition chamber (base pressure $\sim 2 \times 10^{-11}$ Torr) by sequentially depositing high-purity Sb, K, and Cs onto a heated substrate referred to as a ''puck.'' Photocathode #1 was fabricated on April 1, 2011 and photocathode #2 on November 18, 2011. Each photocathode was delivered to JLab within a few days of fabrication, in the manner described below. The constituent sources consisted of high-purity Sb pellets, resistively heated in a tungsten crucible, while the K and Cs sources consisted of SAES alkali dispenser strips [12] for photocathode #1, and Alvatec source vials [13] for photocathode #2. The puck was similar to pucks used at the Continuous Electron Beam Accelerator Facility at JLab for securing GaAs photocathodes [11] but made of aluminum with a thin layer of stainless steel explosion bonded to the top which served as the coating substrate. The substrate must be heated during the photocathode fabrication and, because the heater inside the BNL deposition chamber had modest heating capability, aluminum was chosen for the puck body because it has relatively small mass and good thermal heat conduction. Stainless steel was chosen as the photocathode substrate as previous measurements at BNL indicated it provided high QE at 532 nm [14]. The stainless steel surface was polished using diamond paste with 9 μm grit, cleaned with a citric-acid soap in an ultrasonic bath, rinsed in deionized water and then vacuum baked to 200°C inside a load lock system before insertion into the deposition chamber. Figure 1 shows a photograph of the puck resting in a fork holder composed of BeCu, which was used to translate the puck sequentially over the three deposition sources.

No attempt was made to limit the photocathode active area—the entire stainless steel substrate was coated with photocathode chemicals. The fork and puck could be heated to 150°C and cooled to −80°C, and biased to 5 kV in order to make QE measurements during and after the depositions. A crystal microbalance was used to monitor and control the deposition rate of the Sb and K sources. The following deposition procedure was used: (i) the puck was heated to 100°C and ~14 nm of Sb was applied to the substrate at a rate of ~0.5 nm/s; (ii) the puck temperature was raised to 140°C and 30 nm of K was applied at a rate of ~0.5 nm/s; (iii) the puck was cooled to 135°C, biased at −20 V, and illuminated with ~0.5 mW of 532 nm light; (iv) Cs was applied while monitoring the extracted photocurrent until photocurrent ceased to increase; and (v) the puck was quickly cooled to room temperature.

The QE spectrum of both photocathodes, taken just after reaching room temperature, is shown in Fig. 2. The QE at 532 nm was 0.8% and 2.8% for photocathode #1 and #2, respectively. The QE of photocathode #1 was low because the K dispenser became depleted during fabrication. Additional Sb and Cs was applied in an attempt to increase QE, although in hindsight, these steps were likely not beneficial. Photocathode #1 may have been composed of a mixed state of Cs_3Sb and K_2CsSb. The spectrum for photocathode #2 is more typical for deposition on a stainless steel substrate and the peak QE of both photocathodes was over 20% in the UV. Further information concerning

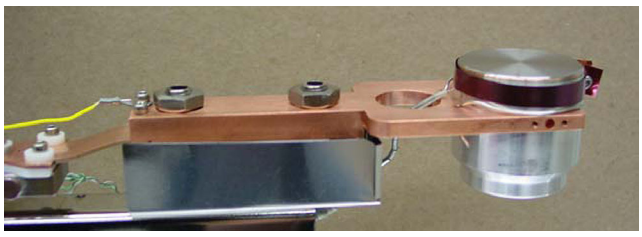

FIG. 1. The transfer arm of the BNL K_2CsSb deposition system holding the stainless steel and aluminum puck. The puck can be biased for QE measurements, heated, and cooled.

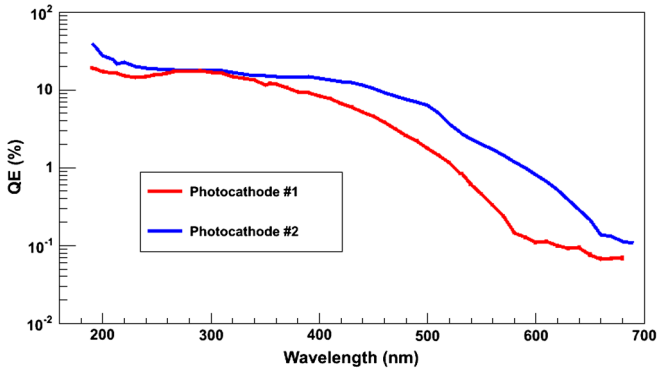

FIG. 2. Spectral response of the K_2CsSb photocathodes created at BNL just after deposition.

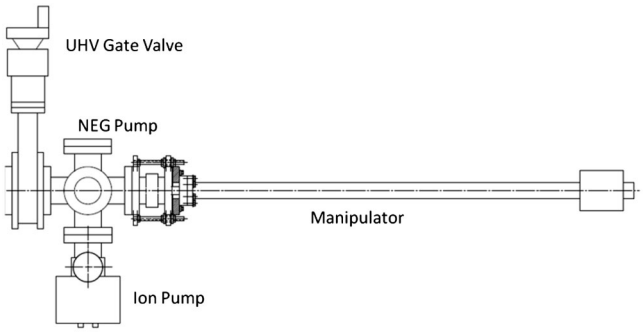

FIG. 3. Schematic of the vacuum suitcase composed of a magnetic sample manipulator, six-way cross with 4.5'' CF, gate valve, and vacuum pumps.

the growth methods and QE spectral measurements can be found in Ref. [14]. Other groups report higher QE at 532 nm, of the order of 8% [2,3], suggesting our growth procedure is not optimized.

B. Transfer the photocathodes to JLab

After fabrication, the puck was pulled from the deposition vacuum chamber and moved into a baked vacuum ''suitcase'' composed of a rotating/translating UHV sample manipulator with ''cradle'' attached to the end to hold the puck, a 4.5 inch six-way Conflat flange (CF) vacuum cross, and an all-metal gate valve opposite the manipulator. A diagram of the suitcase is shown in Fig. 3. A small ion pump (20 $L/s\,N_2$) and NEG pump (600 $L/s\,H_2$) provided pressure $\sim 10^{-11}$ Torr. The cradle grasps the sides of the puck, with the photocathode surface facing perpendicular to the linear motion of the manipulator. Once the puck was installed inside the suitcase, the gate valve was closed and the cradle was then pressed against the back face of the gate valve to prevent the puck from falling out during transit. The trip duration via automobile from BNL to JLab (450 miles) was 10 hours. The pressure inside the suitcase remained at $\sim 10^{-11}$ Torr with occasional intermittent pressures spikes to 10^{-9} Torr when the vehicle encountered bumps in the road. The ion pump was powered during the entire trip.

C. Load lock dc high voltage photogun and diagnostic beam line

Upon arrival at JLab, the vacuum suitcase was attached to a small vacuum cross appended to a gate valve on the GaAs preparation chamber. This vacuum cross was evacuated and baked for 12 hours at 100°C to achieve vacuum $\sim 1 \times 10^{-10}$ Torr. The vacuum within the suitcase did not degrade appreciably during the bakeout of the intervening cross. Following bakeout, the gate valves at the preparation chamber and suitcase were opened, and the K_2CsSb photocathode was quickly transferred first to the preparation chamber and then into the photogun high voltage chamber. Note that the preparation chamber, which normally serves to activate GaAs photocathodes, was not used for this

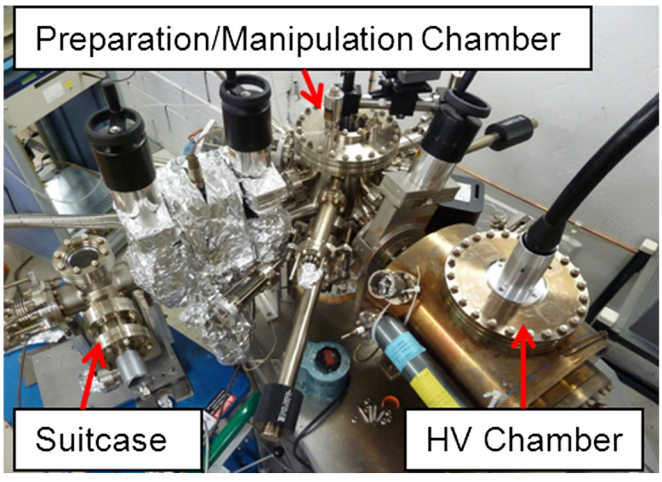

(a)

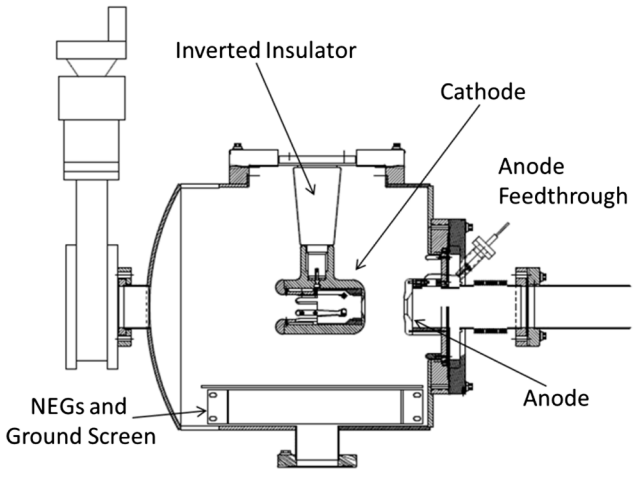

(b)

FIG. 4. Photograph (a) and schematic view (b) of the dc high voltage photogun at JLab.

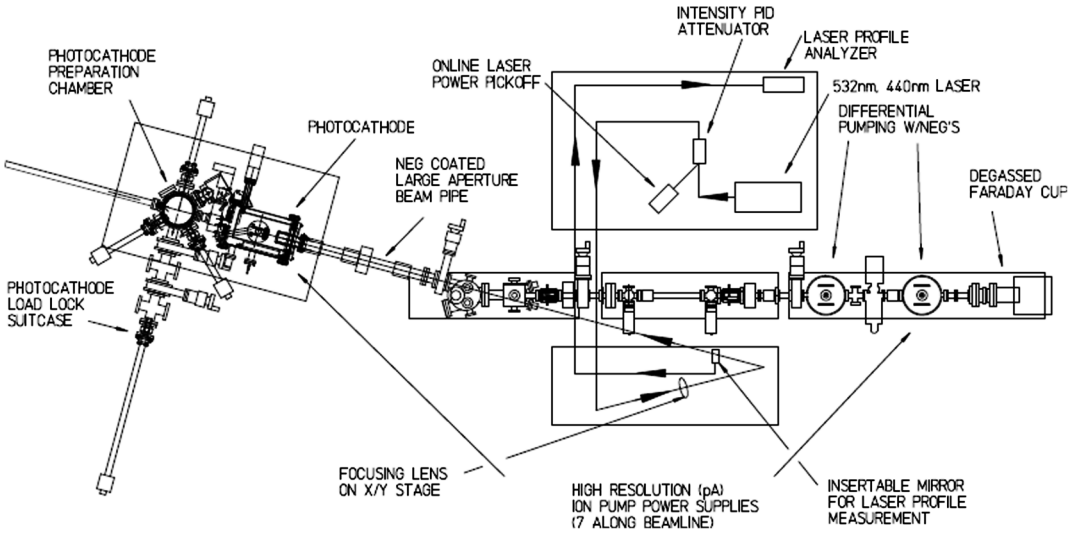

FIG. 5. Schematic of the photogun and beam line at JLab's Injector Test Stand Facility.

experiment. The load locked photogun is depicted in Fig. 4 and described more fully in Ref. [15].

The photocathode was inserted into a large-grain niobium electrode with 25° focusing angle [16]. Photoemitted electrons are accelerated to a kinetic energy up to 200 keV over a 6.3 cm cathode/anode gap. The ring anode is electrically isolated and attached to a sensitive current monitor that detects both field emission and photoemission that does not pass through the anode. The cathode electrode hangs from an alumina insulator (11 cm long) that extends into the vacuum chamber. Ten nonevaporable getter pump modules (SAES WP1250-ST707) surround the cathode/anode gap and provide pressure 2×10^{-12} Torr (uncorrected, N_2 equivalent).

Photoelectrons pass through the anode and are delivered to a water-cooled Faraday cup beam dump ~5 m away. A diagram of the beam line employed is provided in Fig. 5. Solenoid magnets focus the beam and weak steering magnets keep the beam centered in the beampipe. The Faraday cup was baked at 450°C for 24 hours to reduce outgassing at high current. Two differential pumping chambers with NEG pumps serve to vacuum isolate the beam dump from the photogun. Ion pumps with sensitive current monitoring pump inert gasses not pumped by the NEGs and also provide beamloss monitoring along the beam line [17]. In addition, the quality of the beam tune was monitored by x-ray detectors along the beam line and gun chamber.

Beam emittance was determined using the wire scanner technique [18], by measuring the size of the beam using thin wires passing through the beam, for different settings of the last solenoid magnet. A 15° bend and vacuum window provide a means to introduce drive laser light onto the photocathode at normal incidence without requiring mirrors inside the vacuum chamber. Light reflected from the photocathode exits the vacuum chamber via the laser vacuum window within ~0.1° of the incident laser beam.

Two laser systems were used: a frequency-doubled Nd:YVO_4 laser (Coherent Verdi-10) provided up to 4.5 W at the photocathode at 532 nm, and an inexpensive multimode diode laser provided up to 0.2 W at 440 nm. Both lasers were operated in dc mode. Laser power at the photocathode was adjusted via a computer controlled attenuator consisting of a fixed linear polarizer, a rotatable birefringent $\lambda/2$ wave plate, and another fixed linear polarizer. A focusing lens was mounted to x/y stepper motor stages near the laser vacuum window, allowing the laser spot to be positioned anywhere on the photocathode. The 532 nm laser had excellent mode quality and could be tightly focused to 500 μm Gaussian full width at half maximum (FWHM) using a 2 m focal length lens. A larger laser spot (1050 μm) was obtained using a lens with 1.5 m focal length. The spatial mode quality of the 440 nm diode was not nearly as good as the 532 nm laser, and required an anamorphic prism pair to create a relatively uniform spatial profile, which was focused to obtain a nearly spherical Gaussian profile at the photocathode with tightest beam size 1 mm FWHM. A commercial CCD camera and scanning razor-blade apparatus located at the equivalent distance to the photcathode were used to measure laser profile and spot size and verify the laser beam was circular with Gaussian profile. The optical elements (mirrors, wave plates, polarizing cubes) were all purchased with appropriate coatings for the two wavelengths.

The experiment was mostly an exercise in measuring photocathode QE, before, during, and after a particular "run" in which one of the following parameters were varied: elapsed time, beam current, location of the laser beam on the photocathode, laser beam spot size, laser power, laser wavelength, and gun voltage. Photocathode QE could be measured in "real time" while extracting

beam by monitoring the delivered photocurrent to the dump, and the laser power through a calibrated partial reflector. The laser power was also measured by noting the setting of the calibrated laser attenuator. Before and after a run, the QE of the entire photocathode surface was measured by extracting $\sim 1\ \mu$A from the grounded photocathode, with the anode biased at ~ 375 V, while scanning the laser across the photocathode by translating the focusing lens on stepper motor stages. Lasers were left powered throughout the duration of the experiment (and shuttered when beam was not extracted) to minimize laser power drift, which was less than 3% drift over 12 hours. Unless otherwise noted, measurements were made at fixed beam current by continually adjusting the laser power via a software feedback loop that controlled the laser attenuator. The term charge lifetime is defined as the amount of charge that could be extracted from the photocathode before QE fell to $1/e$ of the initial value.

III. RESULTS

A. Initial measurements using K_2CsSb photocathode #1 at 532 nm

The initial QE of photocathode #1 ranged from 0.5% to 0.8% across the 12.8 mm diameter opening of the cathode electrode [Fig. 6(a)]. The QE remained constant for days before extracting beam, suggesting a very long dark lifetime under these vacuum conditions. The photocathode was then biased at 100 kV and charge lifetime measurements were performed at different radial locations at 1 mA beam current. Charge extracted for each run ranged from 6 to 30 C. Following each run, a QE scan was performed [Fig. 6(b)] and an exponential fit was applied to the QE decay. Charge lifetime measurements are plotted in Fig. 7 as a function of radial position of the laser beam relative to the electrostatic center of the photocathode. It was both surprising and disappointing that the charge lifetime of photocathode #1 was comparable to that of GaAs [11]. Furthermore, the charge lifetime was observed to improve as the laser position was moved radially outward, which suggested ion bombardment played a role in QE decay. Namely, ions produced by the beam are preferentially focused toward the center of the photocathode, so by operating with the laser beam displaced from the photocathode center, lifetime is enhanced.

B. Charge lifetime at 440 nm very good; charge lifetime at 532 nm improves

After completing ten lifetime measurements at 532 nm from different radial locations on the photocathode, and repeatedly observing relatively poor photocathode lifetime, lifetime measurements were made using the 440 nm laser. In sharp contrast to previous runs with 532 nm light, charge lifetime of K_2CsSb photocathode #1 was markedly better at 440 nm. In fact, initial runs at 1 mA and 100 and 200 kV gun voltages from the electrostatic center indicated QE only increased with time. Beam delivery from the electrostatic center using a GaAs photocathode is short lived due to ion bombardment [3,11].

While delivering 3 mA beam using a 200 kV bias voltage and the 440 nm laser during an unattended run, a brief power glitch caused three steering magnets to turn off. As a result, beam was missteered into a valve and the flange of a bellows. This condition persisted for

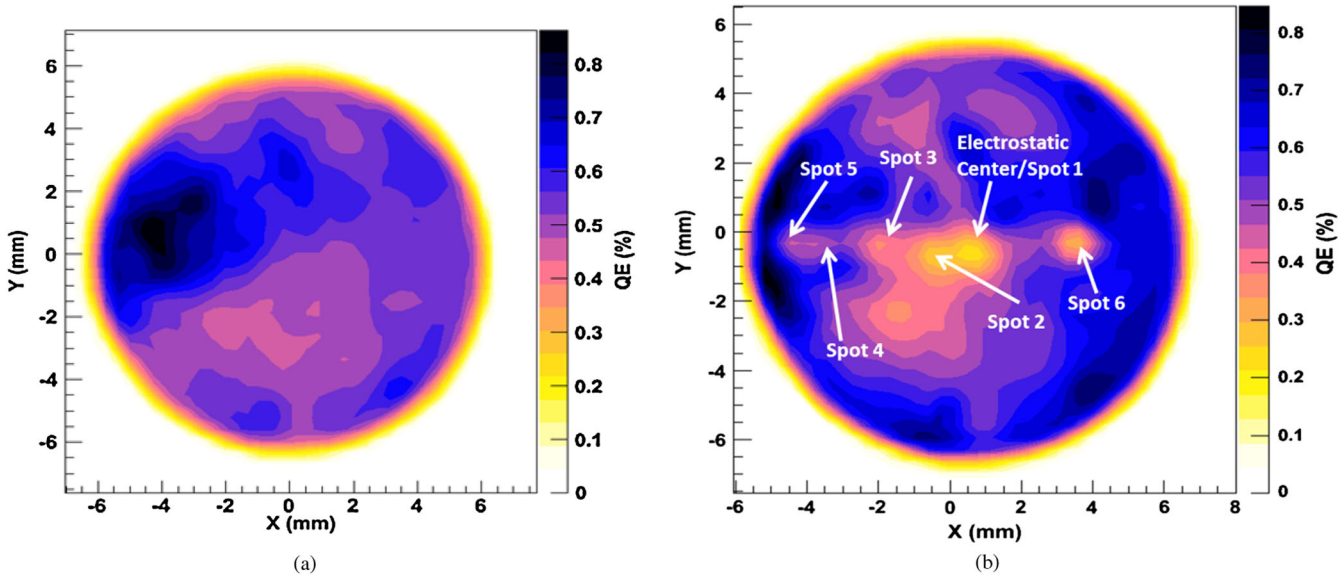

FIG. 6. QE maps of K_2CsSb photocathode #1 using 532 nm light when the photocathode exhibited poor lifetime: (a) before running beam and (b) after running beam from many locations (the numbering denotes the sequential order of the run).

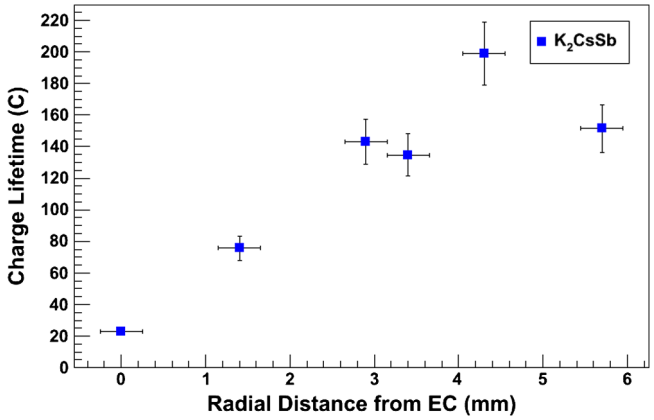

FIG. 7. Charge lifetime of K_2CsSb photocathode #1 versus the radial position of the 532 nm laser spot relative to the electrostatic center of the cathode. The vertical error bars are related to the quality of the exponential fit to the QE decay curves, and the horizontal error bars reflect uncertainty of the laser position relative the electrostatic center.

approximately 1.5 hours, with an increasing amount of beam delivered to the valve, due to the software current lock being enabled. The vacuum at the photogun degraded to $\sim 10^{-9}$ Torr during beam delivery. Fortunately, the beam line was not damaged (i.e., no leak) and vacuum recovered quickly once beam was terminated. The QE was then measured across the entire photocathode at both wavelengths, with a profound reduction in QE observed at the center of the photocathode, but the QE at the edge nearly unchanged, as shown in Fig. 8. Such a vacuum event would have eliminated the QE across the entire surface of a GaAs photocathode.

Following the beam-strike/vacuum event, the charge lifetime of the photocathode at 440 nm was still very good, with QE observed to increase during lengthy runs at current up to 5 mA (the maximum current for the available laser power). Since the center of the photocathode exhibited no QE, beam delivery was from the edge of the photocathode, where efficient transport of the beam is problematic due to an astigmatic imperfection of the cathode/anode electrostatic optic. As a result, a small amount of beam halo intercepts beam line phosphorescent viewers along the beam line, which then charge up and disturb the beam orbit. Eventually, the viewers discharge and orbit recovers. This is evident in Fig. 9(a), where frequent discontinuities in the QE curve are seen. Sharp QE drops correspond to missteered beam at the dump.

After a number of lifetime measurements at 440 nm, beam operations at 532 nm were resumed. In sharp contrast to the initial measurements with 532 nm light, the charge lifetime of the photocathode was greatly improved [Fig. 9(b)]. Higher and higher currents were extracted using 532 nm light with a 500 μm laser spot (FWHM). The QE increased over time at currents up to $\sim$5 mA. The QE was relatively stable at 10 mA beam current and for current $>$16 mA the QE decreased [Fig. 10(a)]. A larger laser spot (1050 μm FWHM) was used to extract beam

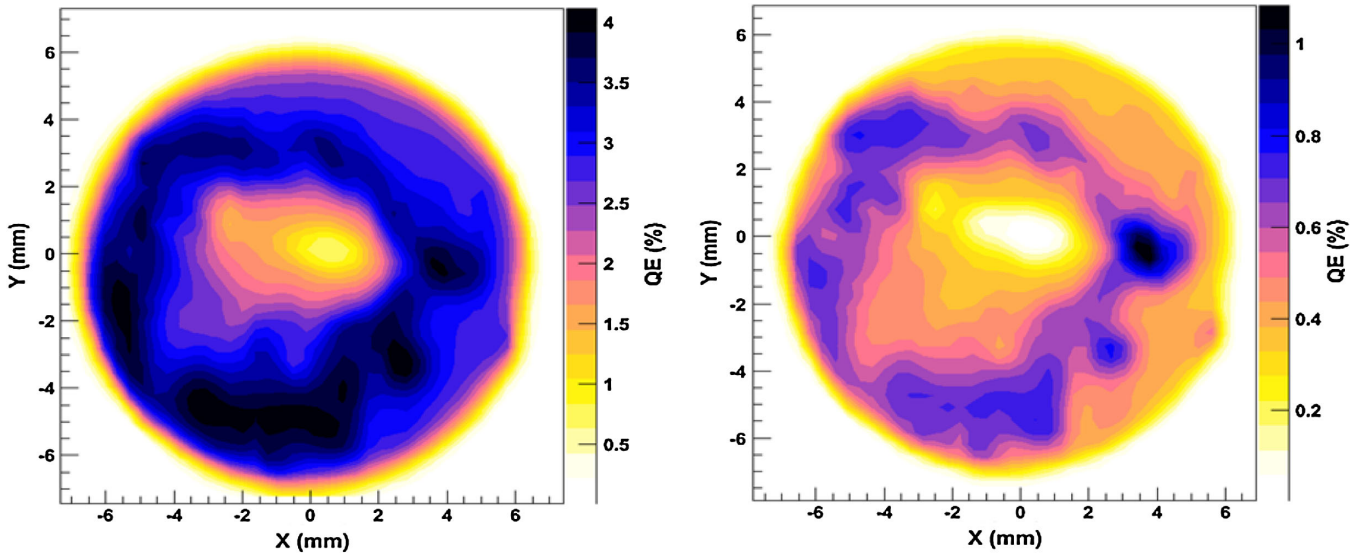

(a) (b)

FIG. 8. QE scans following the vacuum event during which greater than 1.5 mA of beam was dumped into a valve for an extended period of time: (a) 440 nm light and (b) 532 nm light. Absence of QE in the wafer center was an indication that photocathode material was sputtered away by ions produced by the extracted beam. Note the high QE spot in (b) at approximate location $x/y = 4, 0$ mm was produced after extracting 4 mA over 24 hrs using 440 nm light after the vacuum event.

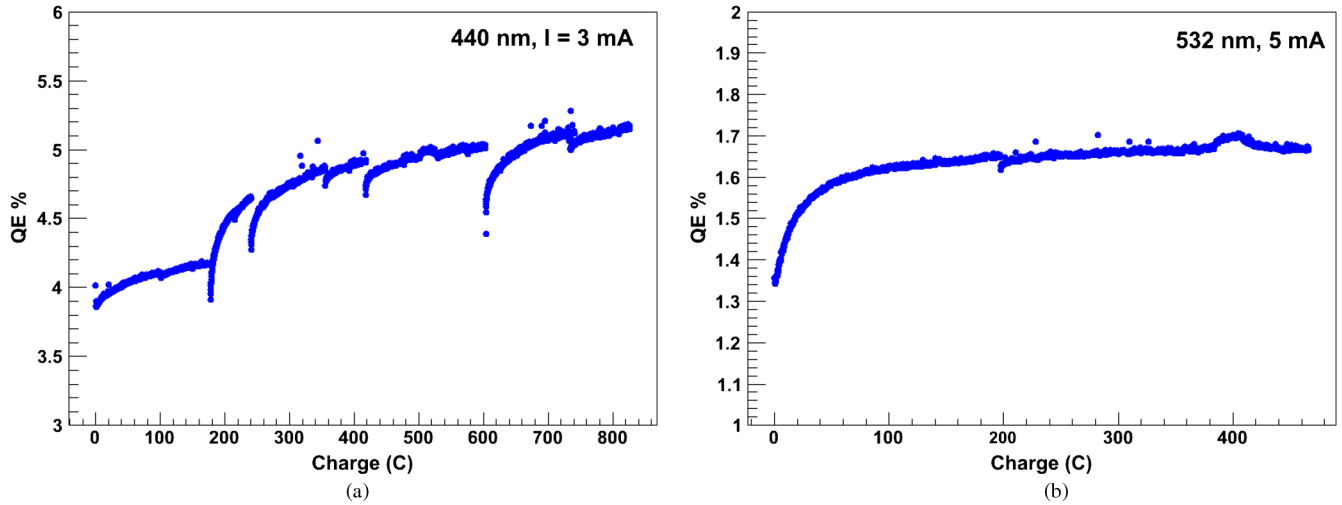

(a) (b)

FIG. 9. QE evolution during 200 kV beam delivery from K_2CsSb photocathode #1: (a) using 440 nm light and (b) 532 nm light. Note QE increasing with extracted charge. The discontinuities are due to static charge buildup on viewers and eventual discharges that move the beam at the Faraday cup.

and the QE was observed to decay more slowly at currents between 15 and 20 mA, corresponding to 17 and 23 mA/mm^2 [Fig. 10(b)].

To explain the QE evolution—in particular, the observed QE increase at low beam currents, the QE decrease at high current, and lifetime enhancement while using a larger laser spot—the QE was monitored without extracting beam, i.e., with a laser illuminating the photocathode but with the photocathode grounded. The QE of the photocathode was mapped before and after laser illumination for a prescribed duration, and then the two data sets were subtracted to create a QE difference map (Fig. 11). There was a slight offset in x/y coordinates that results in imperfect cancellation. For both laser wavelengths, the QE was observed to increase following sustained illumination, with the photocathode at ground potential (i.e., there was no extracted electron beam).

C. K_2CsSb photocathode #2, biased and grounded anode

Photocathode #2 was manufactured without problems and QE was satisfactorily high across the surface, with a value of 2.8% at 532 nm directly after the deposition. Upon arrival at JLab, QE had decreased by nearly a factor of 3. It is not understood why the dark lifetime of this photocathode was so markedly different from photocathode #1.

The central goal assigned to the beam tests with photocathode #2 was to rigorously correlate observed QE evolution with some physical mechanism, in particular, to distinguish between ion bombardment and any chemical changes that might occur due to laser heating. To address this, 10 mA of beam was delivered to the dump using 532 nm laser light positioned at the electrostatic center of the photocathode, while iteratively biasing and grounding the anode electrode during ~1 hour-long intervals.

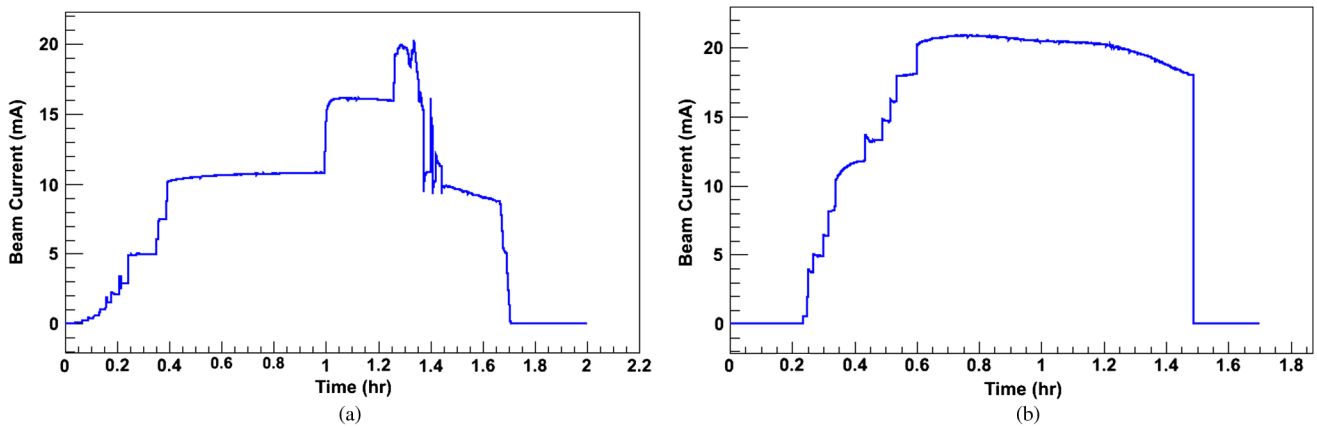

(a) (b)

FIG. 10. Beam current versus time using K_2CsSb photocathode #1 and 532 nm light with laser spot diameter: (a) 500 μm FWHM and (b) 1050 μm FWHM. The larger laser spot provided longer lifetime.

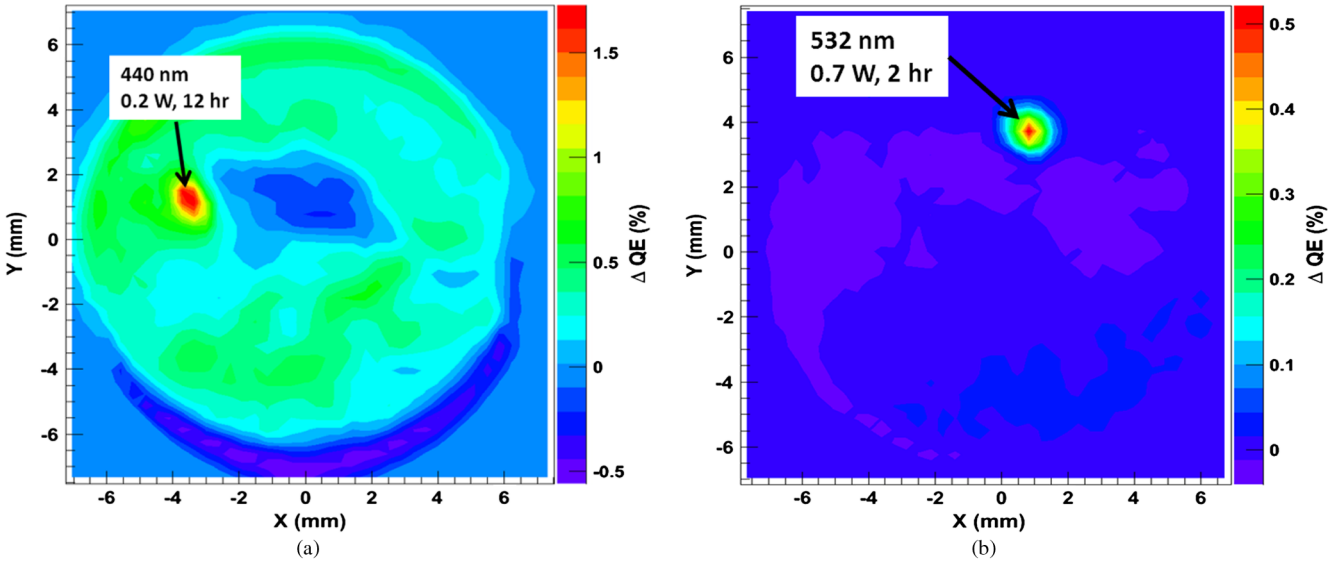

FIG. 11. QE difference scans of K_2CsSb photocathode #1 using (a) 440 nm laser at 0.2 W for 12 hrs and (b) 532 nm laser at 0.7 W for 2 hrs. The photocathode was at ground potential, no beam was extracted while the laser was illuminating the photocathode. The QE increased due to the presence of the laser light, at both wavelengths.

Applying a positive bias to the electrically isolated anode repels ions that are generated downstream of the anode. Previous tests with GaAs indicated that photocathode charge lifetime could be enhanced at the electrostatic center using this technique [11]. As shown in Fig. 12, there was no marked difference in QE decay for the two conditions—anode biased or grounded—suggesting alkali-antimonide photocathodes do not suffer as a result of ion bombardment in an UHV environment.

D. K_2CsSb photocathode #2, laser heating

For the next test, beam was delivered to the dump using 532 nm light at a constant laser power of 0.2 W [1 W/mm^2 (FWHM)], which produced an initial beam current of approximately 1 mA. Beam current was allowed to vary with changing QE. Over a sufficient time period, a clear QE evolution signature was observed. The QE quickly increased from 1.25% to 1.5% in just minutes, and then increased more gradually to over 2% in 5 days [Fig. 13(a)]. The run was eventually terminated, the high voltage turned off, and the photocathode grounded. The laser beam was moved to a fresh photocathode location 1.5 mm away. Laser light at the same power level was reapplied to the photocathode and the QE was measured at low-bias voltage (300 V) at ~2 hour time intervals. The QE at 100 kV was higher than observed at low bias voltage, which is likely due to the Schottky effect. Per [19], considering the photogun cathode/anode geometry, a 100 kV bias voltage provides an electric field enhancement that serves to reduce the threshold energy by 48 meV. Assuming an initial threshold energy of ~2 eV, this level of work function reduction would reasonably provide a ~20% increase in observed QE. Aside from this difference, both conditions resulted in similar QE evolution trends, including the rapid initial QE rise.

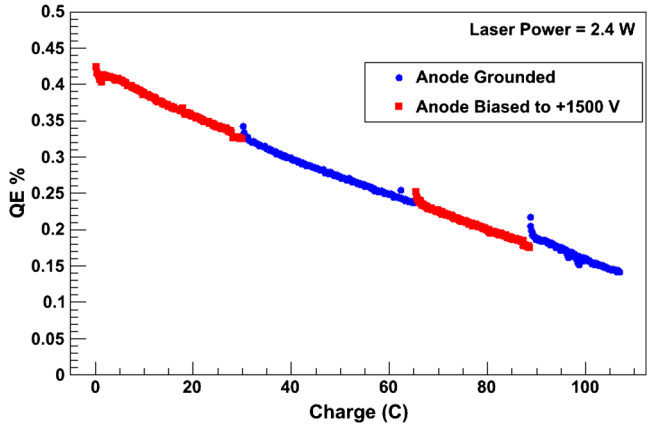

FIG. 12. The QE at the electrostatic center of K_2CsSb photocathode #2 versus extracted charge at 10 mA average current, 100 kV cathode bias voltage, and with the anode biased at +1500 V (red) and grounded (blue)

Again the laser beam was moved to a new location and beam delivered to the dump but this time at higher laser power, ~2 W [10 W/mm^2(FWHM)], corresponding to 10 mA initial beam current. A slight increase in QE was observed during the first hour and then QE fell to a relatively small value over the course of ten hours [Fig. 13(b)]. The discontinuity in the graph at hour 5 was related to a slight missteering of the beam at the dump, likely due to one of the beam line viewers accumulating charge from beam halo. The beam was resteered to the dump without interrupting beam delivery. After ~10 hours, beam delivery was halted, the photocathode grounded, and the laser

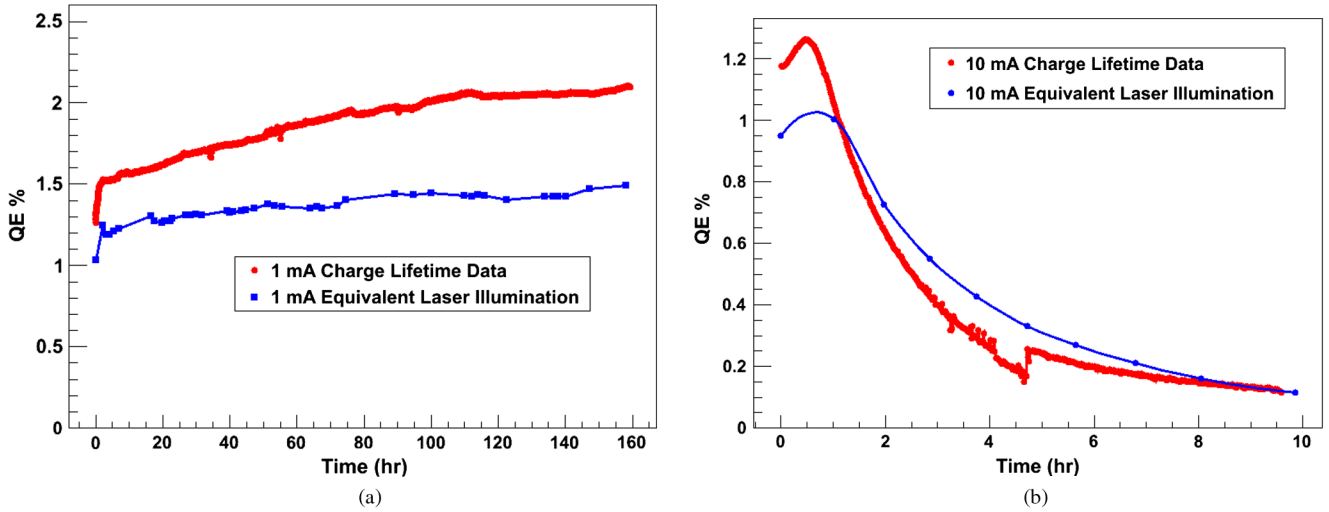

(a) (b)

FIG. 13. QE evolution at (a) 1 mA and (b) 10 mA equivalent laser power. Continuous lines represent QE measured while delivering beam at 100 kV and data points represent QE measured at low voltage during "laser-heating" runs, with no high voltage and no beam delivered to the Faraday cup. Data points were connected to aid the eye.

moved to a fresh location. The QE was measured at 1 h intervals under "no beam" conditions and a similar QE evolution signature was observed. These measurements at high and low laser power/beam current indicate that the QE of K_2CsSb photocathodes varies due to chemical changes induced by the laser, and not due to ion bombardment.

E. Temperature estimates at the illuminated spot

To explain the QE decay of the K_2CsSb photocathodes, estimates of the photocathode temperature were made assuming 65% absorbed laser power (based on optical constants of K_2CsSb and stainless steel [20,21] and using the commercial thermal modeling software ANSYS 14.0 [22]. The thermal analysis included a thin layer of stainless steel (0.8 mm), intervening layers of Cu (0.4 mm) and Ti (0.4 mm) required for the explosion bonding process, the aluminum puck in contact with the niobium cathode electrode, and the alumina inverted insulator. The model assumed excellent thermal contact between all of the components. The grounded end of the insulator, which was welded to a 10 inch stainless steel flange, was anchored at room temperature. A diagram of the thermal model is shown in Fig. 14.

Thermal analysis indicates that practically all of the heat associated with absorbed laser power stays within the thin photocathode and stainless steel layers. This localized

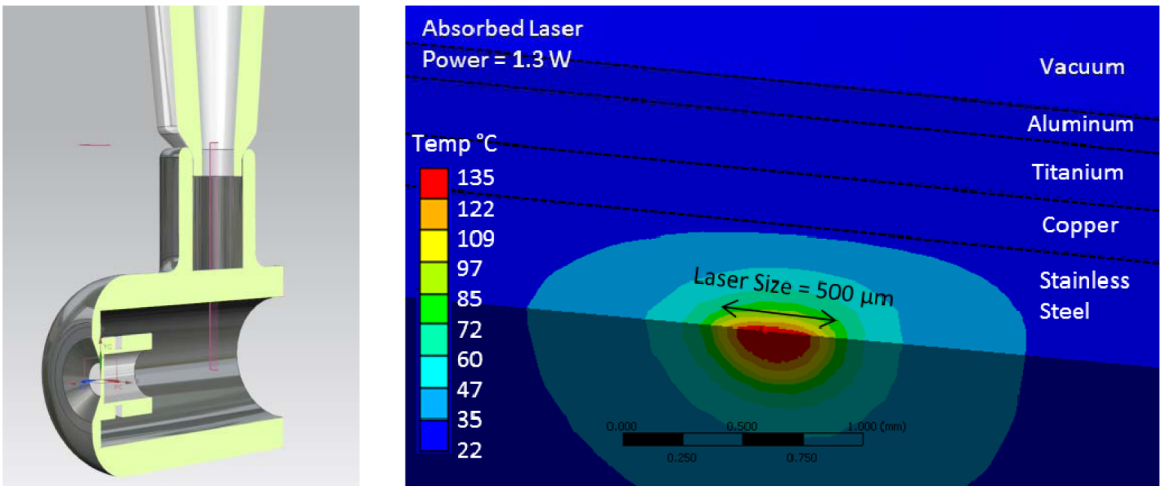

(a) (b)

FIG. 14. (a) Schematic view of the elements used in the ANSYS 14.0 thermal analysis. (b) Close-up cross sectional view of the photocathode and the stainless steel/aluminum puck with 1.3 W of laser light distributed over a 0.5 mm diameter region. The heat is primarily localized within the stainless steel where the temperature reaches 135°C.

TABLE I. Maximum simulated temperature at the illuminated location for a given absorbed laser power for our K_2CsSb/stainless steel/aluminum puck as well as a K2CsSb/molybdenum puck.

	Maximum temperature: Stainless steel substrate and aluminum puck				Maximum temperature: Molybdenum puck		
Absorbed laser power	0.2 W	1.0 W	1.3 W	2 W	1.3 W	3 W	5 W
Laser spot size 0.5 mm	40°C	108°C	135°C	173°C	42°C	67°C	98°C

heating is due to the very poor thermal conductivity of stainless steel. Table I shows the maximum temperature reached for various incident laser powers and for 0.5 mm diameter laser spots. For the two conditions associated with Fig. 13, the thermal model suggests the photocathode reached 40°C and 135°C during the 1 and 10 mA measurements, respectively. We note the QE showed no sign of decrease over 160 hours in the 1 mA measurement, but fell by 80% in just 10 hours during the 10 mA measurement. We speculate there is a temperature threshold, above which chemical changes occur (such as dissociation) that lead to QE loss. A dedicated experiment is required to establish this exact temperature threshold.

For comparison, the same thermal analysis was performed using a molybdenum puck/substrate, which has ~10 times better thermal conductivity than 316 L stainless steel, and it was found that under similar conditions (1.3 W absorbed power), the temperature of the photocathode stays near 40°C, a value empirically determined to be acceptable (i.e., this temperature does not cause the K_2CsSb photocathode QE to decay). For a photocathode with 1% QE, such a laser power level would provide ~10 mA beam current. A photocathode with 12% QE (at 532 nm) grown on a good thermal conductor like molybdenum could provide 100 mA beam current without suffering QE decay associated with laser thermal-induced chemical evolution.

F. Emittance measurements

The geometric rms beam emittance was evaluated for beam produced from both photocathodes as a function of laser wavelength, laser beam size, and photogun bias voltage using the solenoid scan technique [18] from which the normalized rms emittance per laser size was estimated. The field strength of the last beam line solenoid was varied to change the size of the electron beam which was measured using a wire scanner located near the beam dump. Beam widths were extracted from Gaussian fits of the x, y, and u wire signals, with typically ten scans made for each beam condition. A plot of beam width squared as function of solenoid current squared [Fig. 15(a)] provides a measure of beam emittance, as described below.

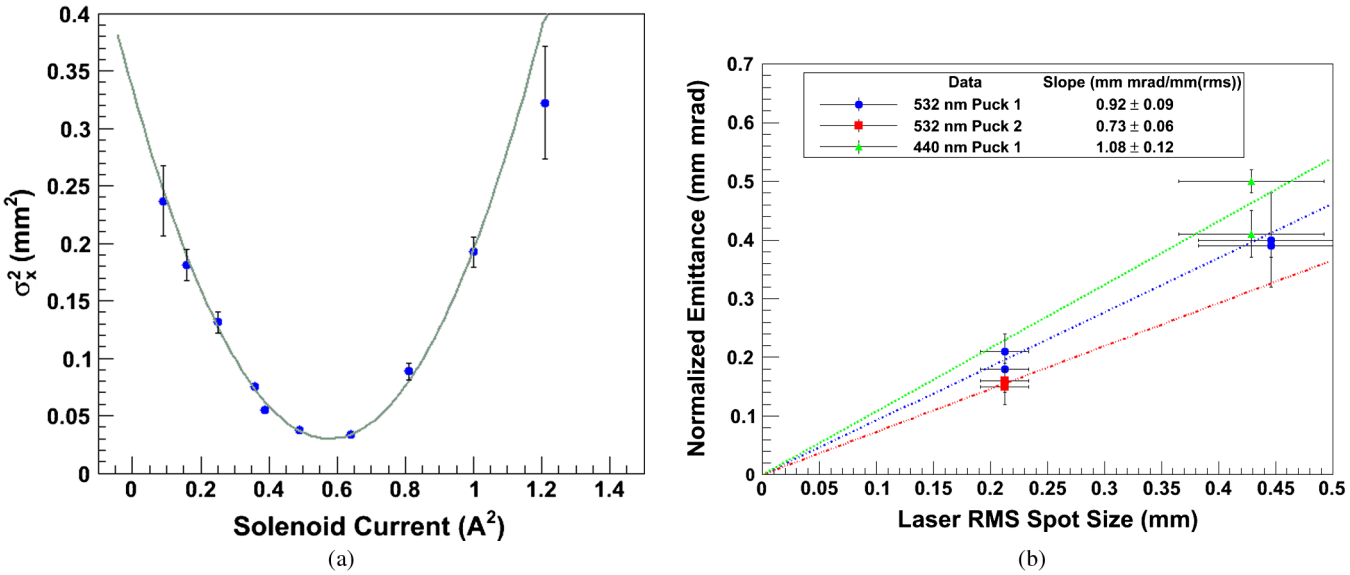

(a) (b)

FIG. 15. (a) Gaussian beam widths in the x direction for different focusing solenoid field strengths, for beam extracted from the electrostatic center of photocathode #2. The data were fit with a parabola to determine emittance, as described in the text. (b) Normalized rms emittance measurements versus laser beam size for measurements performed on photocathodes #1 and # 2. For each photocathode-wavelength configuration, the data were fit with a line through the origin. The slope of the line yields the normalized rms emittance per laser size.

The geometric rms emittance at any given point along the beam line is equal to $\epsilon_{\mathrm{rms}} = \pi\sqrt{\det\ \boldsymbol{\sigma}} = \pi\sqrt{(\sigma_{11}\sigma_{22} - \sigma_{12}^2)}$, where $\boldsymbol{\sigma}$ is the trace space beam matrix at that location. The sigma matrix at the harp, $\boldsymbol{\sigma}_{\mathrm{harp}}$, is defined as $\boldsymbol{R}\boldsymbol{\sigma}_{\mathrm{presolenoid}}\boldsymbol{R}^T$, where $\boldsymbol{R} = \boldsymbol{D}\boldsymbol{Q}$, and $\boldsymbol{D}$ is the transfer matrix

$$D = \begin{bmatrix} 1 & L \\ 0 & 1 \end{bmatrix}$$

with L equal to the drift length between the solenoid and the harp, and

$$Q = \begin{bmatrix} 1 & 0 \\ \frac{-1}{f} & 1 \end{bmatrix},$$

where f is the focusing strength of the solenoid. Here we have assumed the equations of motions are decoupled in the x and y planes. Since the beam radius at the harp (σ_x) is equal to $\sqrt{\sigma_{11,\mathrm{harp}}}$, one can fit the data in Fig. 15 with a parabola of the given form: $\sigma_x^2 = \sigma_{11,\mathrm{harp}} = R_{11}^2\sigma_{11,\mathrm{presolenoid}} + 2R_{11}R_{12}\sigma_{12,\mathrm{presolenoid}} + R_{12}^2\sigma_{22,\mathrm{presolenoid}}$ to extract the beam presolenoid sigma matrix elements and therefore the geometric rms emittance. This was repeated with different laser wavelengths, spots sizes, and beam energies. The normalized rms emittance was calculated using equation $\epsilon_n = \beta\gamma\epsilon_{\mathrm{rms}}$, where β and γ are the usual Lorentz factors due to the relativistic beam. Space charge effects were negligible as dc beam current was kept to $\sim 3\ \mu$A for all measurements.

The normalized rms emittance measurements using photocathode #1 were performed after having completed extensive charge lifetime evaluation and, notably, after the vacuum event which severely reduced QE at the photocathode center. Measurements were made with the laser positioned approximately 2 mm from the electrostatic center and 100 and 200 kV gun bias voltages. Two spot sizes, 500 and 1050 μm FWHM, were used during the 532 nm measurements, while only one spot size, 1010 μm FWHM, was used for the 440 nm measurements. These measurements were plotted versus rms laser beam size and then fit with a line, as shown in Fig. 15(b), where the slope is the normalized rms emittance per laser beam size. The extracted normalized rms emittance per laser rms size was 1.08 ± 0.12 mm mrad/mm(rms) at 440 nm and 0.92 ± 0.09 mm mrad/mm(rms) at 532 nm.

For photocathode #2, consideration was given to evaluating the normalized rms emittance before and after extracting significant charge. In particular, the measurements were performed at the electrostatic center immediately upon installation of the photocathode within the photogun, as well as before and after an extended run at 1 mA (850 C extracted) with a 500 μm FWHM laser spot positioned 2 mm from the electrostatic center, to determine if the normalized rms emittance degraded due to use. For each condition, the normalized rms emittance was the same, within errors. The normalized rms emittance per laser size, shown in Fig. 15(b), was found to be 0.73 ± 0.06 mm mrad/mm(rms) at 532 nm. We did not intend to perform a rigorous thermal emittance measurement; however our normalized rms emittance per laser size values is reasonable considering previously reported thermal emittance values [2]. Emittance measurements are summarized in Table II.

G. Surface morphology

After beam-based measurements, each photocathode was moved via the vacuum transfer suitcase to another building for evaluation of the surface morphology using a scanning electron microscope (SEM) with an energy-dispersive x-ray spectroscopy (EDS) attachment. To reduce the likelihood of photocathode oxidation, an argon-filled gloved bag was used to transfer the samples into the SEM. The transfer took approximately 2 minutes and once inside the SEM, samples were exposed to $\sim 10^{-6}$ Torr vacuum.

1. Photocathode #1

It must be noted that, after performing the charge lifetime measurements described above, photocathode #1 was

TABLE II. Geometric normalized rms emittance measurement summary. Δ EC is the laser spot distance from the electrostatic center. For comparison we have also listed published thermal emittance values [2].

				Normalized rms emittance (mm mrad)				
Δ EC (mm)	λ (nm)	Laser size (FWHM) μm	HV (kV)	Puck 1	Puck 2	Puck 2 after 160 hr, 1 mA	λ (nm)	Thermal emittance (mm mrad/mm(rms)) [2]
0	532	500	100		0.15 ± 0.01		532	0.56 ± 0.03
2	532	500	100		0.16 ± 0.02	0.16 ± 0.02	473	0.69 ± 0.03
2	532	1050	100	0.39 ± 0.02			405	0.87 ± 0.04
2	532	1050	200	0.40 ± 0.08				
3	532	500	100	0.21 ± 0.02				
3	532	500	200	0.18 ± 0.06				
3	440	1010	100	0.50 ± 0.02				
3	440	1010	200	0.41 ± 0.04				

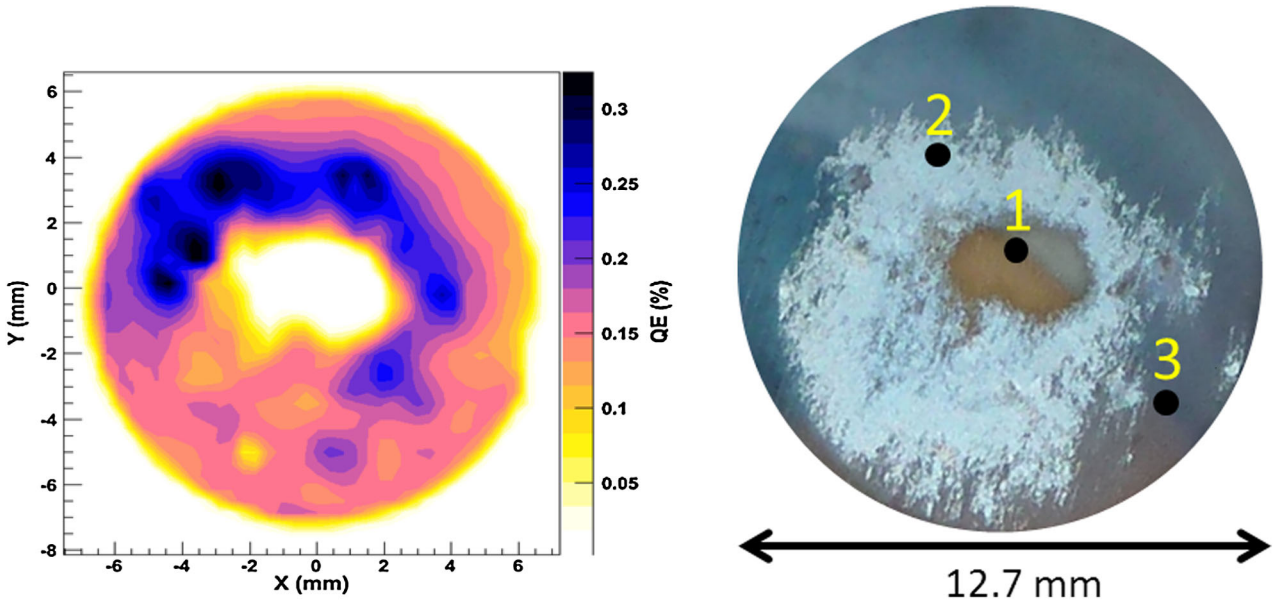

(a) (b)

FIG. 16. (a) QE scan of photocathode #1 prior to transfer to the SEM and, (b) photograph of the photocathode showing the locations evaluated with SEM and EDS.

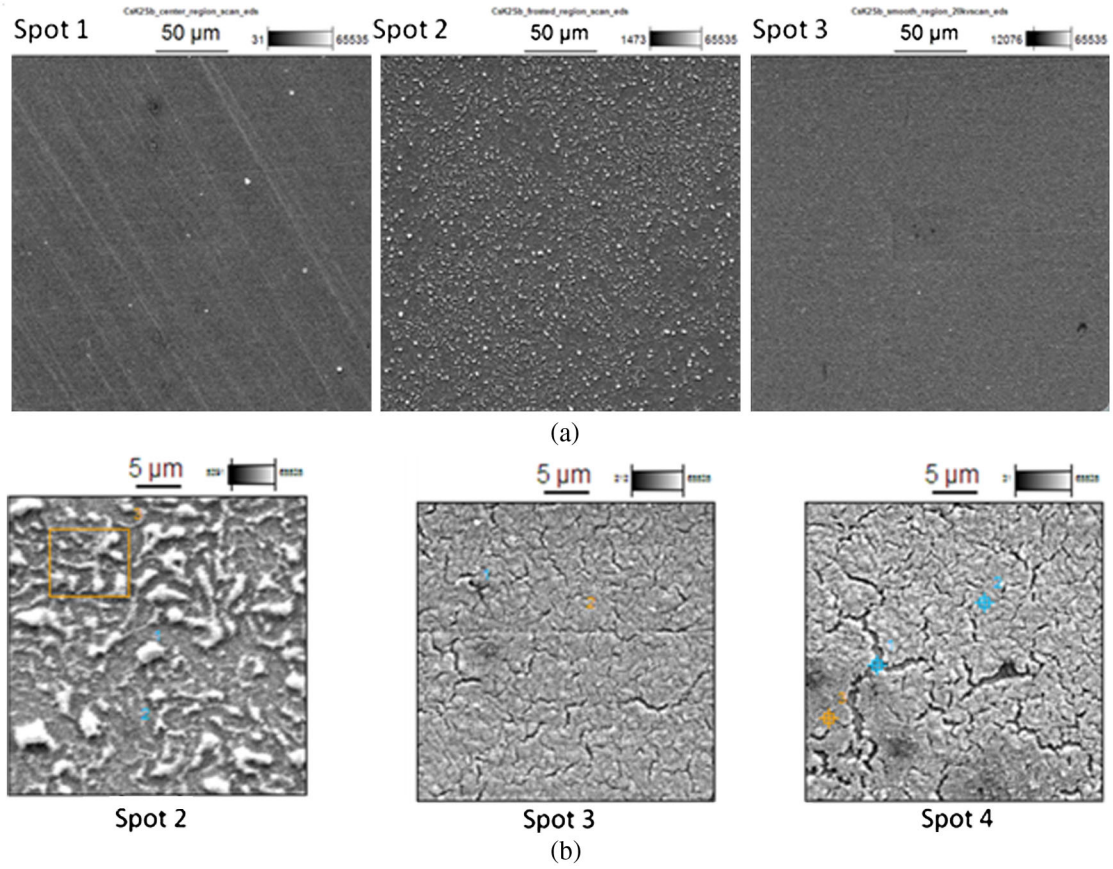

(a)

(b)

FIG. 17. (a) Surface of photocathode #1 at 400x magnification and (b) 3000x magnification.

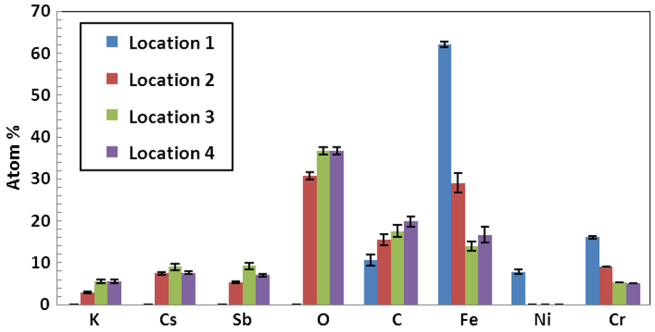

FIG. 18. EDS spectra taken from 400*x* images of locations 1–4 from photocathode #1. Notice location 1 has a purely stainless steel composition.

subjected to global heating inside the photogun high voltage chamber, in a failed attempt to quantify K_2CsSb photcathode lifetime as a function of vacuum level. Specifically, the NEG pumps were heated to approximately 100°C to liberate hydrogen in a relatively controlled manner. An inadvertent consequence was that the photocathode was heated too. In addition, a relatively small amount of Cs (~ one monolayer) was applied to the entire surface in an attempt to restore QE. These activities reduced QE by a factor of 3 [Fig. 16(a)] and likely had some impact on the chemical composition, however surface science evaluation was still deemed worthwhile.

Surface topography and chemical composition were evaluated at four locations using a 10 keV electron beam (Fig. 16), corresponding to the center of the photocathode that suffered nearly complete QE elimination during the vacuum event that occurred when beam was missteered into the beam line, two locations representative of where most of the production beam delivery occurred and a region that was protected behind the cathode electrode [not shown in Fig. 16(b)].

Figure 17 shows images of locations 1, 2, and 3 at 400x magnification and locations 2, 3, and 4 at 3000x magnification. Figure 18 shows the atom percent composition as determined by EDS x-ray data which confirms that location 1 is purely stainless steel, indicating the vacuum event was severe enough to sputter away the entire photocathode layer. Importantly, the rest of the cathode survived this major event, which would have completely destroyed the negative electron affinity surface condition of a GaAs photocathode. The 3000x image of location 2 indicates islands of Cs, K, and Sb (the white flakes), with stainless steel and Sb in between (the darker regions), as compared to locations 3 and 4 which show a more uniform photocathode layer with some cracks exposing the stainless steel substrate
underneath. Interestingly, location 2 still exhibits considerable QE.

2. Photocathode #2

Figure 19 shows a QE scan of photocathode #2 following all beam-based and laser-heating measurements, together with a photograph of the photocathode inside the vacuum transfer suitcase. Visual inspection of the photocathode surface revealed distinct regions corresponding to where beam was extracted, and to where the laser was used to heat the sample without extracting beam. These

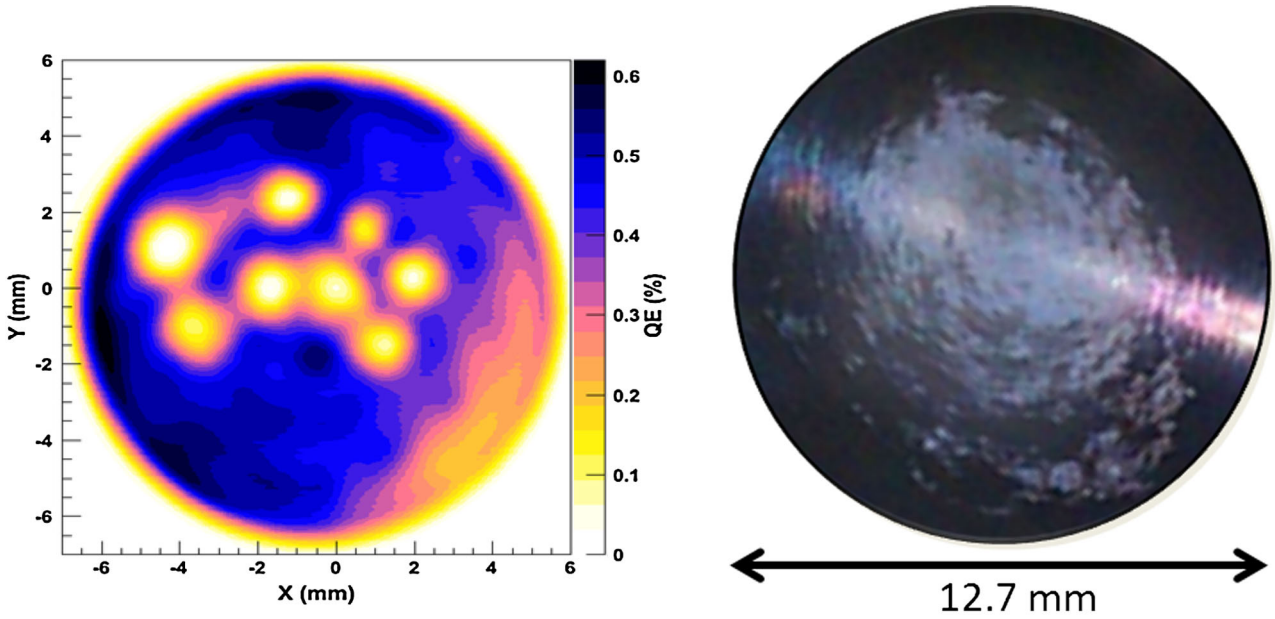

(a) (b)

FIG. 19. (a) QE scan and (b) a photograph of photocathode #2 prior to transfer to the SEM.

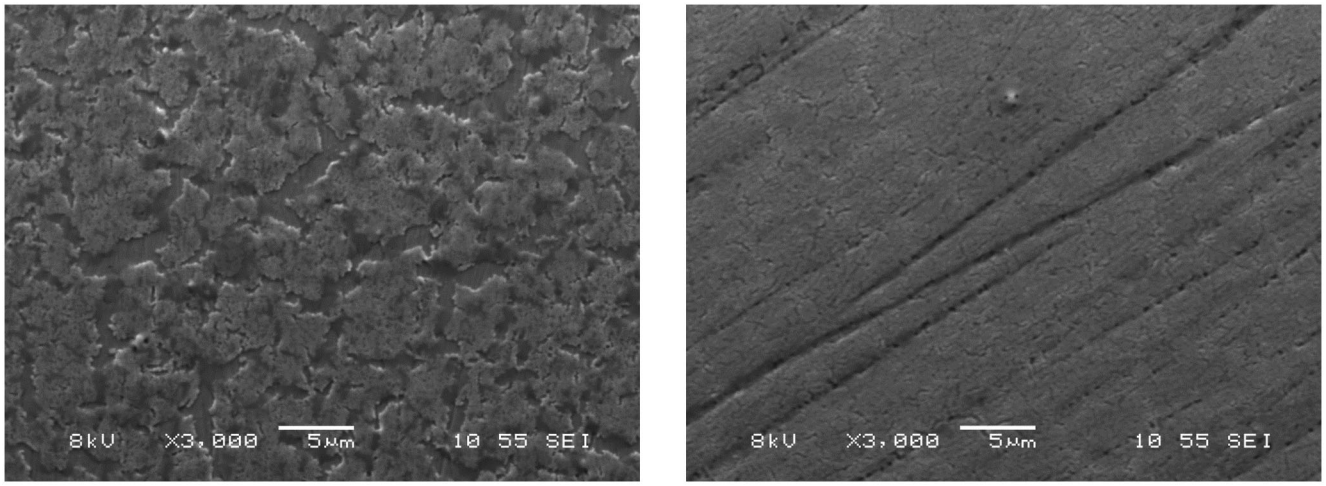

(a) (b)

FIG. 20. SEM images at 3000x magnification using an 8 keV electron beam at photocathode locations that had been illuminated with 2 W laser light, in one case (a) while extracting beam at 10 mA using a laser spot 1050 μm FWHM and the other case, (b) simply heating the photocathode with a laser spot 500 μm FWHM without generating beam. The topology of these two locations was very different, and very different from that of photocathode #1.

distinctive visual markers made it possible to study photocathode regions with known history, to distinguish the characteristics of the photocathode related to beam delivery and laser heating from nominally unused locations.

Problems with the SEM apparatus unfortunately required that the SEM sample volume be vented with air. As a result, the photocathode surface became oxidized before measurements were made. Still, it seems reasonable to comment on the surface morphology. Figure 20 shows 3000x magnification SEM images at two locations that were illuminated with 2 W of 532 nm light, but with different laser spot sizes: (a) 1050 μm FWHM (extracting beam) and, (b) 500 μm FWHM (grounded cathode). It is not certain that the differences in surface morphology are a result of the different laser conditions, but it is reasonable to assume the two locations reached different temperatures.

EDS spectra, shown in Fig. 21, were examined at 400x magnification from these sites and compared to sites nearby that were not illuminated with the laser. The data suggest there is a different amount of photocathode material at each of the three locations. These data provide motivation to perform a dedicated surface science experiment, as discussed earlier, to determine if the QE evolution is associated with the loss of photocathode material due to laser heating.

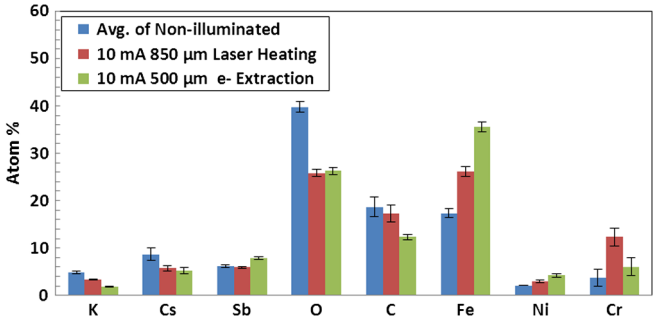

FIG. 21. Chemical assay comparison at locations of photocathode #2 that were illuminated with laser light and from unused locations.

IV. SUMMARY AND CONCLUSIONS

Two K_2CsSb photocathodes were grown at BNL and transported ~450 miles to JLab inside a compact UHV apparatus, where they were installed inside a dc high voltage photogun previously used to evaluate GaAs photocathodes. Charge lifetime measurements were performed at currents up to 20 mA using 532 and 440 nm laser light and at bias voltages of 100 and 200 kV. A total charge of approximately 6000 C was extracted from both photocathodes combined.

Photocathode #1 initially exhibited poor charge lifetime at 532 nm. Charge lifetime at 440 nm was much better, with no observed QE decay at beam currents up to 5 mA over a 24 hours time period. An inadvertent beam steering accident lasting 1.5 hours resulted in the complete removal of photocathode material at the electrostatic center, but left usable photocathode material at the periphery. Subsequent charge lifetime measurements at 532 nm then showed completely different behavior, with markedly improved charge lifetime at milliampere beam currents. It is unclear what aspect of the beam-strike condition resulted in improved photocathode performance from the remaining photocathode material.

Charge lifetime at 532 nm was very good at the outset for photocathode #2 at 1 mA current but poor at 10 mA. Pointed measurements were undertaken to clearly identify QE decay behavior that could be attributed to ion

bombardment. These measurements indicate that under UHV conditions, ion bombardment does not play a significant role in QE evolution. Rather, QE variations appear to be linked to chemical changes associated with laser heating. A thermal model indicates the photocathode grown atop a thin stainless steel substrate can easily reach temperatures exceeding 100°C with just modest laser power (~ 1 W). In hindsight, the stainless steel substrate was a poor choice for high current operations.

Normalized rms emittance was measured using the solenoid scan technique at laser wavelengths of 440 and 532 nm and at 100 and 200 kV bias voltage. The normalized rms emittance values for photocathode #1 were slightly higher than those of photocathode #2, and perhaps this is a result of the harsh vacuum conditions encountered during photocathode #1 evaluation. The measurements performed on photocathode #2 under UHV conditions showed that there was no change in the normalized rms emittance after extracting a significant amount of charge at milliamp currents.

The topography of the two photocathodes following tests inside the photogun was markedly different. In addition, the topography of the individual photocathodes varied drastically across each substrate. Remarkably, even a photocathode with a very rough surface and nonuniform composition still provided reasonable beam.

There exist interesting questions associated with the use of K_2CsSb photocathodes for high current accelerator applications. One such question is: When does ion bombardment matter? Our measurements show that in vacuum environments $\sim 10^{-12}$ Torr, ion bombardment does not play a significant role in the QE evolution of K_2CsSb. However, at higher pressures, such as that created during the beam steering accident ($\sim 10^{-9}$ Torr), the photocathode center was completely sputtered away.

Photocathode surface morphology deserves further study. The surface of both photocathodes was noticeably different following tests inside the photogun (even to the naked eye). Detailed SEM images clearly indicated significant morphological differences between unused regions, locations where beam was extracted, and locations that were merely illuminated with laser light. What are the factors that affect these changes, and when do these morphological changes impact photocathode lifetime and beam quality? Future beam-based experiments will surely serve to improve our understanding of this important photocathode material.

ACKNOWLEDGMENTS

This paper was authored by Jefferson Science Associates under U.S. DOE Contracts No. DE-AC05-84ER40150 and No. KC0407-ALSJNT-I0013 with funding from the DOE Office of High Energy Physics and the Americas Region ILC R&D program. The authors would like to acknowledge Dr. W. Cao and Dr. H. Elsayed-Ali from the Electrical & Computer Engineering department at Old Dominion University for their assistance making the SEM/EDS measurements.

[1] I. V. Bazarov, B. M. Dunham, Y. Li, X. Liu, D. G. Ouzounov, C. K. Sinclair, F. Hannon, and T. Miyajima, Appl. Phys. **103**, 054901 (2008).

[2] I. Bazarov, L. Cultrera, A. Bartnik, B. Dunham, S. Karkare, Y. Li, X. Liu, J. Maxson, and W. Roussel, Appl. Phys. Lett. **98**, 224101 (2011).

[3] D. H. Dowell, S. Z. Bethel, and K. D. Friddell, Nucl. Instrum. Methods Phys. Res., Sect. A **356**, 167 (1995).

[4] K. Aulenbacher *et al.*, Nucl. Instrum. Methods Phys. Res., Sect. A **391**, 498 (1997).

[5] G. D. Cates, V. W. Hughes, R. Michaels, H. R. Schaefer, T. J. Gay, M. S. Lubell, R. Wilson, G. W. Dodson, K. A. Dow, S. B. Kowalski, K. Isakovich, K. S. Kumar, M. E. Schulze, P. A. Souder, and D. H. Kim, Nucl. Instrum. Methods Phys. Res., Sect. A **278**, 293 (1989).

[6] M. J. J. van den Putte, C. W. De Jager, S. G. Konstantinov, V. Ya. Korchagin, F. B. Kroes, E. P. van Leeuwen, B. L. Militsyn, N. H. Papadakis, S. G. Popov, G. V. Serdobintsev, Yu. M. Shatunov, S. V. Shevelev, T. G. B. W. Sluijk, A. S. Terekhov, and Yu. F. Tokarev, AIP Conf. Proc. **421**, 260 (1998).

[7] W. Hillert, M. Gowin, and B. Neff, AIP Conf. Proc. **570**, 961 (2001).

[8] C. Hernandez-Garcia, S. V. Benson, G. Biallas, D. Bullard, P. Evtushenko, K. Jordan, M. Klopf, D. Sexton, C. Tennant, R. Walker, and G. Williams, AIP Conf. Proc. **1149**, 1071 (2009).

[9] L. Cultrera *et al.*, Phys. Rev. ST Accel. Beams **14**, 120101 (2011).

[10] B. Dunham *et al.*, in *Proceedings of the 3rd International Particle Accelerator Conference, New Orleans, Louisiana, USA, 2012* (IEEE, Piscataway, NJ, 2012), MOOAA01.

[11] J. Grames, R. Suleiman, P. A. Adderley, J. Clark, J. Hansknecht, D. Machie, M. Poelker, and M. L. Stutzman, Phys. Rev. ST Accel. Beams **14**, 043501 (2011).

[12] Alkali Metal Dispensers Brochure 1789, SAES getters, 20020 Lainate (MI) Italy (2007).

[13] Alvasource Cromate-free metal vapor sources, Alvatec Alkali Vacuum Technologies GmbH, 9330 Althofen, Austria (2012).

[14] J. Smedley, T. Rao, and E. Wang, AIP Conf. Proc. **1149**, 1062 (2009).

[15] P. A. Adderley, J. Clark, J. Grames, J. Hansknecht, K. Surles-Law, D. Machie, M. Poelker, M. L. Stutzman, and R. Suleiman, Phys. Rev. ST Accel. Beams **13**, 010101 (2010).

[16] M. BastaniNejad, Md. Abdullah Mohamed, A. A. Elmustafa, P. Adderley, J. Clark, S. Covert, J. Hansknecht, C. Hernandez-Garcia, M. Poelker, R. Mammei, K. Surles-Law, and P. Williams, Phys. Rev. ST Accel. Beams **15**, 083502 (2012).

[17] J. Hansknecht, P. Adderley, M. L. Stutzman, and M. Poelker, AIP Conf. Proc. **1149**, 1143 (2009).

[18] B. M. Dunham, Ph.D. thesis, University of Illinois at Urbana-Champaign, 1993.
[19] J. R. Howorth, A. L. Harmer, E. W. L. Trawny, R. Holtom, and C. J. R. Sheppard, Appl. Phys. Lett. **23**, 123 (1973).
[20] D. Motta and S. Schönert, Nucl. Instrum. Methods Phys. Res., Sect. A **539**, 217 (2005).
[21] B. Karlsson and C. G. Ribbing, J. Appl. Phys. **53**, 6340 (1982).
[22] ANSYS®, Release 14.0, ANSYS Inc. (2012).